06

Study of operability of a nonlinear converter based on a $LiGaSe_2$ crystal with surface antireflection microstructures under nanosecond laser excitation

© P.D. Kharitonova[1,2], S.N. Smetanin[1], L.I. Isaenko[2,3], I.V. Smirnov[4], A.A. Sirotkin[1], P.G. Zverev[14], A.G. Papashvili[1], S.I. Lobanov[2,3], A.P. Eliseev[2,3], A.A. Goloshumova[2,3], A.A. Bushunov[2,5], A.A. Teslenko[2,5], V.A. Lazarev[5], M.K. Tarabrin[2,5]

[1] Prokhorov Institute of General Physics, Russian Academy of Sciences, Moscow, Russia
[2] Novosibirsk State University, Novosibirsk, Russia
[3] S.V. Sobolev Institute of Geology and Mineralogy SB RAS, Novosibirsk, Russia
[4] National Research University „Moscow Power Engineering Institute“, Moscow, Russia
[5] Bauman Moscow State Technical University, Moscow, Russia

e-mail: polincharik@ya.ru

Received December 27, 2024
Revised January 25, 2025
Accepted February 28, 2025

Laser-induced damage threshold for $LiGaSe_2$ with different antireflection microstructures and without it by 1-on-1 method using a nanosecond $YAG:Nd^{3+}$ laser with intracavity optical parametric oscillation at a wavelength of $2.1\,\mu$m is investigated. A two-stage optical parametric oscillator based on $KTiOPO_4$ and $LiGaSe_2$ crystals with antireflection microstructures pumped by a nanosecond $YAG:Nd^{3+}$ laser is developed. The results of a numerical and physical experiment on testing a $LiGaSe_2$ crystal with antireflection microstructures as an active nonlinear medium for the parametric conversion of laser radiation into the mid-infrared range are presented.

Keywords: $LiGaSe_2$ crystal, antireflection microstructures, laser-induced damage threshold, parametric conversion, mid-infrared range.

DOI: 10.61011/EOS.2025.03.61159.13-25

Introduction

Wideband coherent mid-infrared (IR) sources with optical parametric oscillation (OPO) are powerful tools for broadband laser spectroscopy [1,2]. This requires the development of efficient nonlinear frequency converters in the mid-infrared range. At present, lithium-containing ternary chalcogenide crystals have proven to be highly relevant as promising nonlinear media for mid-IR photonics because of their broad transmission range and high laser-induced damage threshold (LIDT) [3–8]. Such crystals ($LiGaS_2$, $LiGaSe_2$, $LiInS_2$, and $LiInSe_2$) were comparatively analyzed for frequency conversion of 1-μm and 2-μm lasers into the mid-IR range [5]. It has been shown that using pumping at a wavelength of 2-μm for OPO in a nonlinear $LiGaSe_2$ crystal can provide significantly more broadband IR output emission (~ 3000 nm) than using pumping at wavelength $1\,\mu$m (~ 300 nm). This is attributable to the specificity of the refractive index dispersion of this crystal. $LiGaSe_2$ is also characterized by a relatively high second-order nonlinear coefficient (~ 10 pm/V), a very wide transmission range ($0.37-13.2\,\mu$m) and a moderate LIDT (0.45 J/cm^2) at a wavelength of $1.06\,\mu$m, 5.6 ns [9,10].

At the same time, the issue of reducing the reflection losses from the crystal surfaces for such broadband radiation is acute, since the refractive index of $LiGaSe_2$ is $n \approx 2.3$ in the wavelength range of $2-12\,\mu$m, and the Fresnel losses from each crystal surface in the mid-IR range are about 16%. The solution is to create special antireflection microstructures (ARM) on the crystal surface for ensuring broadband antireflection [11]. This approach for laser crystals has shown the advantage of higher LIDT compared to the standard approach of applying broadband antireflection interference coatings [12]. Previously, ARM have been applied not only to laser crystals [12,13] but also to nonlinear GaSe crystal at wavelengths longer than $\lambda_{dif} \approx 4\,\mu$m [14,15]. The minimum antireflection wavelength, estimated to be [13] $\lambda_{dif} \approx np$ (where p is the period of the microstructure) can be reduced by applying a smaller value of p to ensure pumping of the laser in the range of $2\,\mu$m. Recently, such ARM with a 2-micron edge were successfully fabricated on the surface of a nonlinear $LiGaSe_2$ crystal [16]. It is now important to determine the laser-induced damage threshold when pumping this crystal at wavelength of $2\,\mu$m both in the presence and absence of ARM, and to test the performance of $LiGaSe_2$ with antireflection microstructures as active nonlinear media for OPO in the mid-IR range.

The laser-induced damage threshold of $LiGaSe_2$ crystals with and without antireflection microstructures at wavelength of $2.128\,\mu$m with a pulse duration of 7.2 ns was compared by testing in this study. The results of testing of $LiGaSe_2$ crystal with antireflection surface microstructures as an active nonlinear medium for parametric conversion of

laser radiation into the mid-IR range are also presented for the first time.

Material

Single crystals $LiGaSe_2$ (LGSe) of optical quality were grown. Crystals were grown using a modified Bridgman-Stockbarger method under low temperature gradients [16]. Polished plane-parallel optical elements with a given orientation were fabricated from the obtained crystals for further studies: $\Theta = 90°$, $\varphi = 39°$. The orientation is chosen for the phase-matching type II of the form 1730 (e)$\rightarrow$ 2764 (o) + 4625 (e), where the numbers correspond to wavelengths in nanometers, (o) — an ordinary wave polarized perpendicular to the crystallo-optic plane XY, (e) — extraordinary wave polarized in the crystallo-optic plane XY. Some of the fabricated samples were used to create antireflection microstructures on the surface.

For LGSe crystals with a certain orientation, irrespective of the growth technique, characteristic fluctuations of transmittance values as a function of wavelength are inherent, which is attributable to a less homogeneous bulk structure with the presence of small inclusions. With this in mind, the modes of ARM generation were modified to maximize transmittance in the range from 2 to 10 μm. The obtained transmission spectra of LGSe with and without ARM were demonstrated in Ref. [16]. When ARM is generated, pronounced absorption bands near 3 and 6 μm appear on the transmission spectra of LGSe, which are attributed to O–H bond vibrations [17]. Lithium-containing chalcogenide crystals are subjected to post-growth high-temperature annealing in a special atmosphere to improve the transmittance. Therefore, annealing of samples with ARM in selenium atmosphere was used to reduce the above absorption. Since the products of the laser ablation effect on the crystal substance remain on the modified surface, the samples were washed in solvents in several stages before annealing. This allowed for removal of the surface contamination.

Another approach to absorption reduction was realized in experiments on variation of treatment modes during laser ablation. The developed method for creating antireflection microstructures on crystal surfaces utilizes laser ablation to precisely remove material and create microscopic craters of a given depth and diameter. The material removed by ablation from the surface in the form of droplets, vapor and solid fragments is ejected at supersonic speeds from the ablation zone into the space above the crystal, after which a fraction of the material is deposited on the sample surface in the area around the ablation zone. An ablation zone blowing system is used to eliminate this phenomenon: pressurized air is blown directly to the area in focus of the lens. A stream of compressed air displaces the plume of ablated material so that deposition of material occurs at a considerable distance from the ablation region — outside the working surface of the crystal. As a further development of the solution with elimination of excessive moisture in the atmosphere in the ablation zone, a system of blowing with compressed nitrogen was realized.

Measurement of laser-induced damage threshold of $LiGaSe_2$ with and without antireflection microstructures at wavelength of 2.128 μm

LIDT was tested using a developed YAG:Nd^{3+} laser with transverse diode pumping and electro-optical Q-switching at a wavelength of 1.064 μm with degenerate OPO in a $KTiOPO_4$ (KTP) crystal at a wavelength of 2.128 μm [18]. Stabilization of the laser operation at wavelength of 2.128 μm at a spectral line width of 1 nm was accomplished by installing the KTP converter in a copper block with a Peltier temperature controller at 25°C. The laser output pulse energy was fixed at 10 ± 0.1 mJ at a wavelength of 2.128 μm with a pulse duration of 7.2 ± 0.1 ns. During the experiment, the energy of the radiation pulse was changed using variable transmission filters based on a set of colored optical glass samples. The radiation was focused on the studied sample using a lens with a focal length of 75 mm. The beam radius at the focus (in the plane of the test sample) was measured using the Foucault knife-edge method at the $1/e^2$ level, which was 537 μm along the horizontal axis and 483 μm along the vertical axis. The optical resistance of the samples was measured by the „1-on-1“ (1-on-1 test) method corresponding to GOST R 58370-2019 (ISO 21254-2:2011) „Optics and Photonics. Lasers and laser-related equipment. Methods for determination of laser-induced damage threshold. Part 2. Threshold determination“.

Two LGSe samples with antireflection microstructures on each of them (sample 1 and sample 2), and two samples without ARM (sample 3 and sample 4) were used as the studied samples. Samples were cut in the phase-matching direction ($\Theta = 90°$, $\varphi = 39°$). The size of the samples was $7 \times 7 \times 2$ mm. Two antireflective microstructures (ARS 1.1 and ARS 1.2), each measuring 2×2 mm, were applied to sample 1 to both (input and output) front faces of the crystal (7×7 mm), with microstructure periods of 1.0 and 1.1 μm, respectively. Two antireflection microstructures (ARM 2.1 and ARM 2.2) measuring 2.2×3.9 mm and 3.5×2.6 mm with microstructure periods equal to 0.8 and 0.9 μm, respectively, were applied to sample 2. Two more samples (sample 3 and sample 4) — without ARM.

Measurements of the LIDT of the samples were carried out in 2 stages — preparatory and finishing. During the preparatory stage, the necessary conditions for the final experiment were determined on Sample 1 (in the vicinity of ARM 1.1); the required pulse energy level near the laser damage threshold and the permissible distance between adjacent irradiation sites on the sample, which is bounded

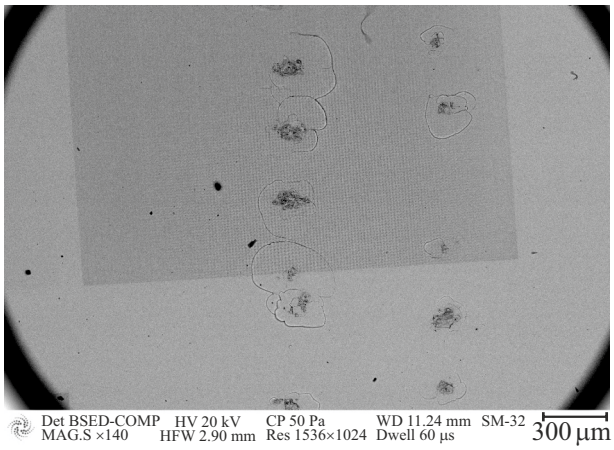

Figure 1. Photograph of sample 1 in the vicinity of the ARM 1.1 microstructure after exposure.

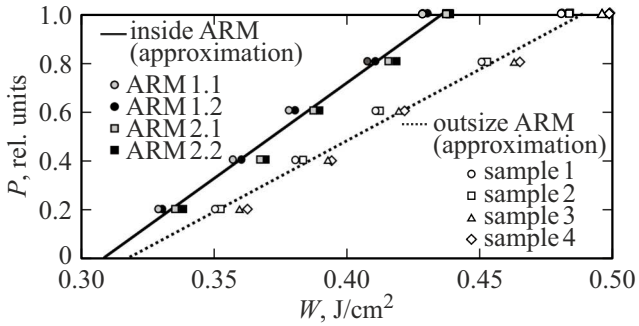

Figure 2. Dependence of the breakdown probability on the radiation energy density: ARM 1.1 (or ARM 1.1) is the first microstructure of the sample *1*; ARM 1.2 (or ARM 1.2) is the second microstructure of the sample *1*; ARM 2.1 (or ARM 2.1) is the first microstructure of the sample *2*; ARM 2.2 (or ARM 2.2) is the second microstructure of sample *2*; sample 1 and sample 2 are samples *1* and *2* without microstructures; sample 3 and sample 4 are samples *3* and *4* without microstructures.

below by the mutual influence of impact acts and above by the transverse size of the microstructure.

In the final stage, measurements were performed on a series of samples with obtaining of statistically significant results. The best results of comparative measurements were obtained for samples with ARM partially covering their surface, which provided measurement of the optical breakdown threshold both in the ARM area and outside it without changing the sample.

It was found in the preparatory stage that when the distance between the irradiation sites is at least $H = 330\,\mu$m with a optical breakdown probability less than $P = 1.0$, the mutual influence of neighboring impact acts can be neglected. Fig. 1 shows the measurements in the preparatory phase.

The photograph shows a square microstructure of ARM 1.1 with size 2×2 mm on the surface of sample 1 after exposure to laser pulses with energies of 3.3 mJ (right vertical row of dots) and 3.5 mJ (left vertical row of dots). Five irradiation sites are placed in a row within the microstructure with $H = 330\,\mu$m. All irradiation sites within the microstructure were damaged in the left row — probability of breakdown $P = 1.0$. One of the points within the microstructure is not breached in the right row, i.e., the probability of breakdown $P = 4/5 = 0.8$, so a pulse energy of 3.3 mJ (corresponding to an energy fluence of 0.41 J/cm^2) is chosen as the initial one for the finishing stage of the experiment on a series of samples.

Next, the finishing stage of the experiment was carried out, where the dependences of the optical breakdown probability P on the fluence of the radiation pulse W for a series of samples were found. The obtained dependences with their linear approximations for a series of samples and microstructures in them are shown in Fig. 2.

As a result of statistical processing of measurements performed inside the microstructures, the following threshold values of radiation energy fluence were obtained: $W_0 = 0.31$ J/cm^2, $W_{0.5} = 0.37$ J/cm^2, and $W_1 = 0.44$ J/cm^2 at breakdown probabilities $P = 0$, 0.5 and 1, respectively, i.e. the breakdown damage by half probability can be defined as $W_{0.5} = 0.37$ J/cm^2 with a determination error of plus or minus $(W_1 - W_0)/2 = 0.07$ J/cm^2. The following threshold fluence values were obtained outside the microstructures: $W_0 = 0.32$ J/cm^2, $W_{0.5} = 0.40$ J/cm^2, and $W_1 = 0.49$ J/cm^2 at optical breakdown probability $P = 0$, 0.5 and 1, respectively, i.e. the damage threshold by half probability can be defined as $W_{0.5} = 0.40$ J/cm^2 with a determination error of plus or minus $(W_1 - W_0)/2 = 0.09$ J/cm^2. Thus, the LIDT of the microstructures of $LiGaSe_2$ crystals was found to be as high as for $LiGaSe_2$ crystals without them. The difference in values is within the error of determination.

The present measurement results at wavelength of $2.128\,\mu$m (7 ns) can be compared with the previously obtained LIDT measurement result at wavelength of $1.064\,\mu$m (6 ns) for LGSe crystal without ARM, which was 0.4 J/cm^2 [19], which is in agreement with the obtained values of $W_{0.5} = 0.37 - 0.40$ J/cm^2 at half the optical breakdown probability ($P = 0.5$) in LGSe crystals with and without ARM.

Two-stage parametric light generator on KTP and LGSe crystals

A $LiGaSe_2$ crystal with aperture of 5×5 mm and length 7 mm cut in the phase-matching direction ($\Theta = 90°$, $\varphi = 39°$) was used as the tested active element. Antireflection microstructures were applied to both planar parallel polished faces (5×5 mm) of the crystal to increase the transmittance of the LGSe crystal from 68% to $T_{LGSe} = 75\%$ for the signal wave at wavelengths in the range 2764–2418 nm, generated in OPO, where an idler wave with a difference frequency at wavelengths in the range should also be generated 4625–8866 nm under the

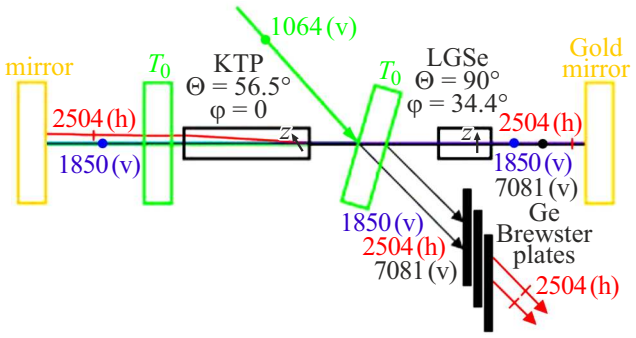

Figure 3. Optical scheme of two-stage OPO on KTP and LGSe crystals: crystallooptic axes Z of KTP and LGSe crystals are oriented in the horizontal plane (figure plane); (v) — vertical polarization of radiation; (h) — horizontal polarization of radiation.

action of parametric pumping at wavelengths in the range 1730−1900 nm (transmittance of LGSe crystal in this range amounted to 60−67%), previously obtained by OPO in KTP crystal under the action of laser pumping with the initial wavelength of 1064 nm. Therefore, a KTP crystal with an aperture of 5 × 5 mm and length 20 mm, cut in the direction $\Theta = 58°$, $\varphi = 0°$, with plane-parallel polished ends without antireflection coatings (microstructures) is also used in the present work. The transmittance of the KTP crystal for the signal wave (2764−2418 nm) was $T_{KTP} = 82\%$. A nanosecond YAG:Nd^{3+}-laser was used as a laser pumping source with a fundamental wavelength of 1064 nm and a spectral width of 0.15 nm with electro-optical Q-switching of the resonator with a radiation pulse energy of 25 mJ, pulse duration of 10 ns, beam quality factor $M^2 = 2.3$ with a pulse repetition frequency of 2 Hz.

Thus, it was necessary to realize a tunable two-stage wavelength conversion of laser radiation first from 1 μm to 2 μm in the KTP crystal, and then from 2 μm further to the mid-IR range (> 5 μm) in the LGSe crystal. We propose for this purpose an original scheme of a two-stage single-resonator OPO on KTP and LGSe crystals with a single resonator, high-Q for the wave (2764−2418 nm), which is the signal wave in both KTP and LGSe crystals. Then the wave (1730−1900 nm) will be an idler wave in KTP, and the wave (4625−8866 nm) is an idler wave in LGSe.

The proposed optical scheme of the two-stage OPO is presented in Fig. 3. Here, the generation of a signal wave with a length of 2504 nm in two processes simultaneously is shown as an example: 1) 1064 (v)→2504 (h) + 1850 (v) in the KTP crystal ($\Theta = 56.5°$, $\varphi = 0°$); 2) 1850 (v)→2504 (h) + 7081 (v) in the LGSe crystal ($\Theta = 90°$, $\varphi = 34.4°$). The brackets indicate the direction of polarization of the interacting waves in the laboratory coordinate system: (v) — vertical, (h) — horizontal. The idler wave (1850 nm) of the first process is the pump wave of the second process. Since the generated extraordinary wave (2504 nm) in the KTP crystal experiences beam walk-off, a counter-propagating pump configuration is used for the first crystal (KTP) with the pump wave (1064 nm) directed opposite to the waves entering the second crystal (LGSe). This compensates for the walk-off of the input waves (1850 nm and 2504 nm) in the LGSe crystal. The high-Q resonator is formed by gold-sputtered mirrors that are highly reflective for all generated waves.

To couple the laser pump, protect the gold mirrors (which have low laser-induced damage threshold), and shield the LGSe crystal (opaque at 1064 nm), as well as to enable double-pass pumping of the KTP crystal, the setup incorporates a pair of intracavity interference mirrors. These mirrors are sputtered on CaF_2 substrates (transparent in the IR range up to 9000 nm) and are highly reflective at the pump laser wavelength of 1064 nm, while maintaining high transmission of $T_0 = 94\%$ in the wavelength ranges of 1730−2764 and 4625−8866 nm. To selectively detect the generated signal wave (2504 nm) at the output of the converter, a germanium Brewster plate stack was installed, transmitting horizontally polarized radiation at the 2504 nm wavelength. The stack was retracted for detection of the total output radiation. To study the contribution of the LGSe crystal to the generation of the signal wave (2504 nm), it was removed from the setup.

This setup does not have the element of effective output of the generated radiation. To record the radiation, it is extracted via reflection from both surfaces of one of the intracavity mirrors (each surface has a low reflectivity of 3%). The setup will be optimized in the future for more efficient IR output, but this will increase the generation threshold due to an increase in the useful loss coefficient.

This setup is of interest due to the highest resonator Q-factor, allowing the lowest generation threshold. The generation threshold is further reduced by decreasing the radius of the laser pump beam (at focusing) and decreasing the length of the OPO resonator. The minimum radius of the pump beam is determined by walk-off of the extraordinary wave (2504 nm) after passing a 20 mm long KTP crystal, which is 0.9 mm. The length of the resonator is technically limited from below to 80 mm, corresponding to the tightest packing of optical elements in the setup.

Predictive modeling of the two-stage OPO was performed in the SNLO software product. Since the calculation program describes a single converter, the simulation was divided into two stages: 1) crystal KTP — active, crystal LGSe — passive, 2) crystal LGSe — active, crystal KTP — passive. For the active crystal, both its nonlinear optical characteristics and transmission coefficient were taken into account, while for the passive one - only the transmission coefficient. The losses contributed by all mirrors were taken into account. Laser pumping parameters (1064 nm) — pulse energy 25 mJ, pulse duration 10 ns, and beam radius varied (as well as the length of the OPO resonator) in the first step were considered. The output parameters of the calculation in the first stage (for wavelengths 1850 and 2504 nm) were the input parameters of the calculation in the second stage.

Calculations at the first stage have shown that in order to increase the conversion efficiency, it is reasonable to use the tightest packing of optical elements with reduction of the resonator length to $L = 80$ mm, and it is necessary to choose the smallest pump beam radius ($r = 0.9$ mm) equal to the value of the walk-off of the extraordinary wave in the KTP crystal. The initial calculation results (at optimal lengths of $L = 80$ mm and $r = 0.9$ mm) show that the KTP crystal generates two-micrometer radiation with pulse energies of 0.90 mJ and 0.66 mJ at wavelengths of 1850 nm and 2504 nm, respectively.

In the second calculation stage (in LGSe crystal), radiation with pulse energies of 0.16, 1.32, and 0.08 mJ at wavelengths of 1850, 2504, and 7081 nm was obtained at the converter output, respectively. Fig. 4 shows these computational results on a time scale. It can be seen that adding an active LGSe crystal to the setup should result in a two-fold (1.32 mJ/0.66 mJ) amplification of the signal wave (2504 nm) at the converter output. In this case, the share of output radiation corresponding to the signal wave (2504 nm) increases approximately two-fold — from 42% to 85% - when the active LGSe crystal is added. The conversion efficiency from the original laser pumping wave (1064 nm) to the longest idler wave (7081 nm) is here estimated to be 0.3% (0.08 mJ/25 mJ) with a quantum efficiency 2%. The conversion efficiency is expected to be increased in the future by optimizing the output optical element of the setup.

Two-stage OPO generation on KTP and LGSe crystals was experimentally studied taking into account the modeling results. The output radiation spectrum were measured using MDR-2 monochromator with PbS-photodetector PDA30G-EC and pulse energies of individual spectral components

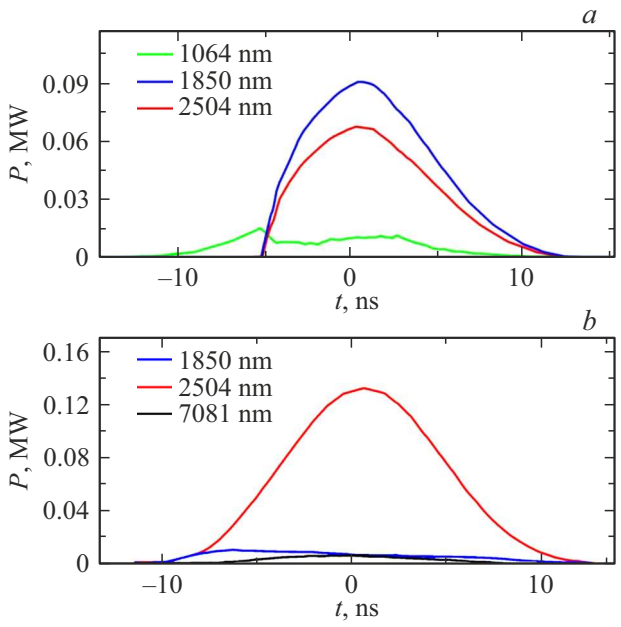

Figure 4. The simulation results of the two-stage OPO: (*a*) — conversion in KTP in the first calculation stage; (*b*) — conversion in LGSe in the second calculation stage.

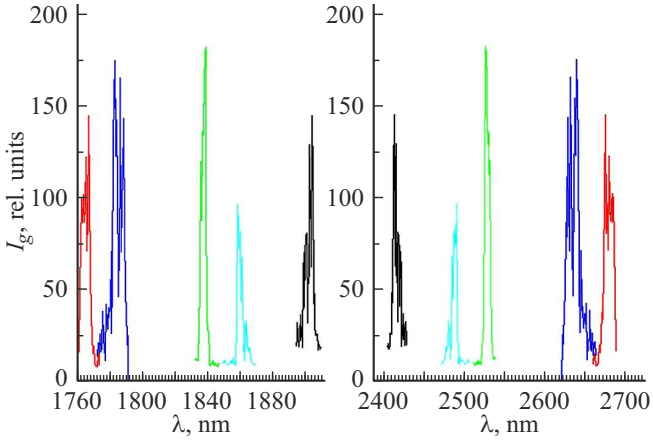

Figure 5. The obtained spectra of the tunable output 2-μm radiation: red lines — pair 1766 and 2677 nm; blue lines — 1784 and 2636 nm; green lines — 1838 and 2527 nm; blue lines — 1858 and 2490 nm; black lines — 1900 and 2418 nm.

by power and energy meter Ophir with pyroelectric sensor PE50BB-DIF-C. As expected, the most efficient generation was obtained in the shortest resonator ($L = 80$ mm) and with the smallest beam radius ($r = 0.9$ mm). Rotating the KTP and LGSe crystals in the phase-matching plane allows tuning the wavelengths of the output radiation. Fig. 5 shows the results of wavelength tuning of parametric generation of 2-μm radiation obtained by rotating the KTP crystal under the action of laser pumping (1064 nm, 25 mJ, 10 ns) in the presented OPO setup (Fig. 3). Under the action of laser pumping (1064 nm), the tunable generation of signal and idler waves in KTP crystal in the tuning ranges 1766−1900 and 2636−2418 nm was experimentally realized. The difference frequency generation for these waves realized in the LGSe crystal provides a wavelength range of tunable IR radiation 5351−8869 nm.

During experimental implementation of parametric generation at 1850 nm and 2504 nm wavelengths (with the corresponding rotation angles of KTP and LGSe crystals), as in the performed modeling, the pulse energy was measured for the combined output radiation (1850 nm+ 2504 nm + 7081 nm) (without the germanium Brewster plate stack in the setup) and separately for the signal radiation (2504 nm) (with the germanium Brewster plate stack in the setup) both in the presence and in the absence of the LGSe crystal in the setup.

The following experimental results were obtained. In the setup containing both crystals (KTP and LGSe), the pulse energy of the combined output radiation (1850 nm + 2504 nm + 7081 nm) was measured at 0.42 mJ, while the pulse energy of the signal wave (2504 nm) alone was 0.33 mJ. Thus, the signal wave accounted for 79% of the total output radiation, which shows reasonable agreement with the second-stage modeling result of 85%. Rotating the LGSe crystal away from the phase-matching condition resulted in a decrease of the signal wave's share in the output radiation.

When the LGSe crystal was removed from the setup, the pulse energy of the total output radiation (1850 nm + 2504 nm) was strongly increased to 1.03 mJ due to the reduction of the extraneous losses contributed by the LGSe crystal before ($T_{LGSe} = 75\%$). However, the pulse energy of the signal wave (2504 nm) weakly increased to 0.36 mJ, so the proportion of the signal wave in the output radiation decreased to 35%, which is in reasonable agreement with the result of the first stage of simulation — 42%. The energy of the pulse with a wavelength of 7081 nm could not be measured; it does not exceed the level of 0.01 mJ (0.08 mJ in the model) —at the limit of the sensitivity of the meter. However, the observed increase of the fraction of the signal wave (2504 nm) in the output radiation in the presence of the LGSe crystal, which is consistent with the simulation results, proves the successful operation of the LGSe crystal as an active crystal of a two-stage OPO with a single signal wave.

Conclusion

$LiGaSe_2$ crystals with large aperture and high optical quality were grown in this study. They were cut and polished in an orientation suitable for down-conversion from $2\,\mu$m wavelength. Antireflection microstructures on both polished surfaces were fabricated using optimized femtosecond laser ablation, which provided a antireflection effect over a wide wavelength range of $2-10\,\mu$m.

Comparative tests of the LIDT under the action of a nanosecond YAG:Nd^{3+} laser with intracavity parametric light generation at the wavelength $2.1\,\mu$m with a pulse duration of 7.2 ns by the 1-on-1 method for various surfaces with ARM and for a polished surface without ARM have been carried out. The damage threshold of the microstructures of $LiGaSe_2$ crystals was found to be as high as for $LiGaSe_2$ crystals without them. The difference in values is within the error of determination. The present measurement results at the wavelength of $2.128\,\mu$m (7 ns) can be compared with the previously obtained damage threshold measurement result at the wavelength of $1.064\,\mu$m (6 ns) for $LiGaSe_2$ crystal without microstructures, which was 0.4 J/cm^2 [19], which is in agreement with the obtained values $W_{0.5} = 0.37-0.40$ J/cm^2 at half probability of breakdown ($P = 0.5$) in $LiGaSe_2$ crystals both with and without microstructures.

A setup model has been developed for two-stage parametric light generation in KTP crystals when pumped by a nanosecond YAG:Nd^{3+} laser and $LiGaSe_2$ with antireflection microstructures. The results of theoretical calculation of the experiment with the resonator configuration corresponding to the developed model in the SNLO software product are presented. This setup is of interest due to the highest goodness of the resonator, allowing the lowest generation threshold. In the future, the setup will be optimized for more efficient IR output, but this will increase the generation threshold due to an increase in the useful loss factor.

Two-stage OPO generation on $KTiOPO_4$ and $LiGaSe_2$ crystals was experimentally studied taking into account the modeling results. As expected, the most efficient generation was obtained in the shortest resonator ($L = 80$ mm) and with the smallest beam radius ($r = 0.9$ mm). The tunable generation of signal and idler waves in the $KTiOPO_4$ crystal in the tuning ranges of 1766−1900 and 2636−2418 nm was experimentally implemented under the action of laser pumping (1064 nm). The difference frequency generation for these waves realized in the $LiGaSe_2$ crystal provides the wavelength range of tunable IR radiation of 5351−8869 nm. An increase of the fraction of signal wave in the output radiation in the presence of $LiGaSe_2$ crystal was observed in the result of the experiment, which is consistent with the simulation results and proves the successful operation of $LiGaSe_2$ crystal as an active crystal of two-stage OPO with a single signal wave.

Funding

This work was supported by RNF, project № 20-72-10027-P.

Conflict of interest

The authors declare that they have no conflict of interest.

References

[1] G. Ycas, F.R. Giorgetta, E. Baumann, I. Coddington, D. Herman, S.A. Diddams, N.R. Newbury. Nat. Phot., **12** (4), 202−208 (2018). DOI: 10.1038/s41566-018-0114-7
[2] L. Maidment, Zh. Zhang, Ch.R. Howle, D.T. Reid. Opt. Lett., **41** (10), 2266−2269 (2016). DOI: 10.1364/OL.41.002266
[3] W. Cai, A. Abudurusuli, C. Xie, E. Tikhonov, J. Li, Sh. Pan, Zh. Yang. Adv. Funct. Mater., **32** (23), 2200231 (2022). DOI: 10.1002/adfm.202200231
[4] L. Isaenko, L. Dong, A. Kurus, Zh. Lin, A. Yelisseyev, S. Lobanov, M. Molokeev, K. Korzhneva, A. Goloshumova. Adv. Optical Mater., **10** (24), 2201721 (2022). DOI: 10.1002/adom.202201727
[5] L. Zhou, O. Novak, M. Smrz, T. Mocek. J. Opt. Soc. Am. B, **39** (4), 1174−1185 (2022). DOI: 10.1364/JOSAB.454372
[6] M. Namboodiri, Ch. Luo, G.H. Indorf, J.H. Buss, M. Schulz, R. Riedel, M.J. Prandolini, T. Lampann. Optics Continuum, **1** (5), 1157−1164 (2022). DOI: 10.1364/OPTCON.451879
[7] I.O. Kinyaevskiy, A.V. Koribut, L.V. Seleznev, Yu.M. Klimachev, E.E. Dunaeva, A.A. Ionin. Optics and Laser Technology, **169**, 110035 (2024). DOI: 10.1016/j.optlastec.2023.110035
[8] M. Jelínek, M. Frank, V. Kubeček, O. Nová k, J. Huynh, M. Cimrman, M. Chyla, M. Smrž, T. Mocek. In: *2023 Conference on Lasers and Electro-Optics Europe & European Quantum Electronics Conference* (Munich, Germany, 2023). DOI: 10.1109/CLEO/Europe-EQEC57999.2023.10232202
[9] L.I. Isaenko, A.P. Yelisseyev. Semicond. Sci. Technol., **31**, 123001 (2016). DOI: 10.1088/0268-1242/31/12/123001

[10] S.N. Smetanin, M. Jel?nek, V. Kubeček, A.F. Kurus, V.N. Vedenyapin, S.I. Lobanov, L.I. Isaenko. Opt. Mater. Express, **10** (8), 1881–1890 (2020). DOI: 10.1364/OME.395370
[11] D.H. Raguin, G.M. Morris. Appl. Opt., **32** (7), 1154–1167 (1993). DOI: 10.1364/AO.32.001154
[12] D. Hobbs, B. MacLeod, E. Sabatino, S. Mirov, D. Martyshkin, M. Mirov, G. Tsoi, S. McDaniel, G. Cook. Opt. Mater. Express, **7** (9), 3377–3388 (2017). DOI: 10.1364/OME.7.003377
[13] A.A. Bushunov, M.K. Tarabrin, V.A. Lazarev, V.E. Karasik, Y.V. Korostelin, M.P. Frolov, Y.K. Skasyrsky, V.I. Kozlovsky. Opt. Mater. Express, **9** (4), 1689–1697 (2019). DOI: 10.1364/OME.9.001689
[14] A.A. Bushunov, A.A. Teslenko, M.K. Tarabrin, V.A. Lazarev, L.I. Isaenko, A.P. Eliseev, S.I. Lobanov. Opt. Lett., **45** (21), 5994–5997 (2020). DOI: 10.1364/OL.404515
[15] A.P. Yelisseyev, L.I. Isaenko, S.I. Lobanov, A.V. Dostovalov, A.A. Bushunov, M.K. Tarabrin, A.A. Teslenko, V.A. Lazarev, A.A. Shklyaev, S.A. Babin, A.A. Goloshumova, S.A. Gromilov. Opt. Mater. Express, **12** (4), 1593–1608 (2022). DOI: 10.1364/OME.455050
[16] A.A. Teslenko, A.A. Bushunov, L.I. Isaenko, A.A. Shklyaev, A.A. Goloshumova, S.I. Lobanov, V.A. Lazarev, M.K. Tarabrin. Opt. Lett., **48** (5), 1196–1199 (2023). DOI: 10.1364/OL.480758
[17] V.F. Kokorina. Glasses for Infrared Optics (CRC press, Boca Raton, 1996).
[18] I.V. Smirnov, P.G. Zverev, A.A. Sirotkin. J. Physics: Conf. Series, **2494**, 012008 (2023). DOI: 10.1088/1742-6596/2494/1/012008
[19] J.-J. Zondy, V. Vedenyapin, A. Boyko, D. Kolker, L. Isaenko, S. Lobanov, N. Kostyukova, A. Yelisseyev, V. Petrov. Laser Phys. Lett., **13**, 115401 (2016). DOI: 10.1088/1612-2011/13/11/115401

Translated by A.Akhtyamov